Phase lags from multiple flux curves of OH/IR stars

Langevelde, H.J. van; Heiden, R. van der; Schooneveld, C. van

Astron. Astrophys. 239, 193–204 (1990)

ASTRONOMY AND ASTROPHYSICS

Phase lags from multiple flux curves of OH/IR stars

H.J. van Langevelde, R. van der Heiden and C. van Schooneveld

Sterrewacht Leiden, P.O. Box 9513, NL-2300 RA Leiden, The Netherlands

Received November 2, 1989; accepted May 3, 1990

Abstract. We present a method to extract the phase lag from time series of calibrated OH 1612 MHz spectra. The phase lag (τ_0) is the difference in travel time between emission from the front and back of the circumstellar shell.

The phase lag τ_0 is determined from independent phase lag estimates $\hat{\tau}_{ij}$ between the flux curves of various pairs of spectral channels under the assumptions of spherical symmetry and saturated masering. Regardless of how we estimate the interchannel lags τ_{ij}, we derive a weighting scheme to combine them, provided we know their variances. Under simplifying conditions we can analyze this problem algebraically. This yields insight in the structure of the problem and in the limitations for monitor programs to measure the phase lag.

In practice we deal with observations that do not allow these simplifications and we use simulations to establish the weighting scheme. The implementation of our algorithm is described and is presented as a block diagram. A specific form of the interchannel lag estimator is described and we discuss how the parameters for the simulations are obtained. Finally, new data from the Dwingeloo telescope are merged with historic data to give new values for the phase lags of the shells around OH/IR stars from the Dwingeloo sample (Herman and Habing, 1985a).

Under several assumptions we combine the value of the phase lag with angular radii from the literature to derive distances to several stars. These distances slightly differ from earlier ones, based on the same method, and have more reliable errors on them. We present the bolometric luminosities for the stars that have accurate distances.

Key words: masers – numerical methods – stars: OH/IR – stars: circumstellar matter – distances

1. Introduction

1.1. OH/IR stars

The two-peaked galactic masers observed in the satellite line of OH at 1612 MHz originate in circumstellar shells around highly evolved stars (Goldreich and Scoville, 1976; Reid et al., 1977; Olnon, 1977). According to this model the characteristic double peaked spectrum is maser emission from the steadily outflowing OH, amplified with greatest efficiency in the directions of maximum coherent path length. Hence the blue- and redshifted peaks are the emission from the near and far cones of the shell.

Send offprint requests to: H.J. van Langevelde

Apart from interstellar UV, responsible for the dissociation of water molecules into OH, the phenomenon is believed to be dominated by the physical conditions of the star. A large mass loss rate is required, not only to provide enough OH, but also to form a thick dust shell. This is essential because it is believed that the population inversion of the OH molecules is pumped by IR emission (Elitzur et al., 1976) that is provided by the dust. The dust absorbs the radiation from the star and reradiates it in the far IR. Indeed, all double peaked OH masers coincide with an IR source that quite often is optically thick. Then no optical counterpart is seen and these objects are known as OH/IR stars (see Herman and Habing, 1985a, or Jones, 1986, for a review).

Most of these stars are variable. In fact, Mira's sometimes show the effects described above and it is quite clear that OH/IR stars and Mira's are closely related, the Mira's having a dust shell that does not yet obscure the star. As the output of the star varies, so will the IR from the dust shell. Indeed IR variability is observed for several sources. This implies that the maser emission, if present, will also vary.

An important observational fact is that the masers and the infrared emission show variations with the same characteristics. For several objects it is reported that the variability follows the IR variations accurately (Harvey et al., 1974; Engels et al., 1983). This clue tells us that the masers are saturated, i.e. that all inverted OH molecules are used in the maser process. On a macroscopic scale this means that the maser will follow the IR input linearly.

If we monitor the OH flux spectrum accurately we can measure phase lags, i.e. the time shifts between the flux curves from different parts of the OH spectrum. To the observer the blueshifted spectral peak from the front has its maximum before the redshifted peak from the back (see Fig. 1), because the shell is several tens of lightdays across. This back to front phase lag will be denoted by τ_0 and is measured in days. This difference yields the distance between parts of the shell if we multiply its value by the speed of light. The phase lag has been measured for several bright 1612 MHz masers (Schultz et al., 1978; Jewell et al., 1980; Herman and Habing, 1985b). Typical values are 25 lightdays, or $6\,10^{14}$ m, in good agreement with calculations for the chemical composition of outflowing material (Netzer and Knapp, 1987).

This simple model predicts that observations with sufficient resolution reveal rings of emission with increasing radius close to the stellar velocity. Indeed this has been found (Booth et al., 1981; Herman et al., 1985; Diamond et al., 1985 and others). These rings are usually not complete, but they do show that the emission originates in a shell. Large departures from the shell model have been found in sources with an irregular spectrum (e.g. Chapman, 1988).

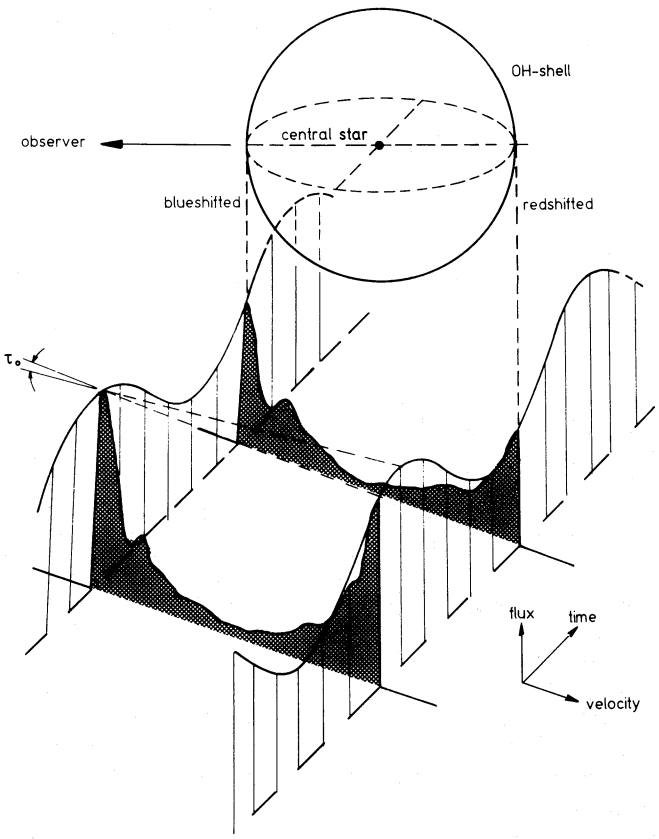

Fig. 1. Schematic view of how the phase lag appears to the observer. The emission originates in the circumstellar shell and the characteristic two-peaked spectrum is observed through the Doppler shift. The spectrum varies in time

Extending the assumptions of this model, the phase lag has been used to determine the distances to some of these stars, by comparing the phase lag to the angular size.

1.2. The outline of this paper

The multichannel phase lag estimation problem is treated in Sects. 2, 3 and 4. Under simplifying assumptions we derive an analytical solution of the estimation problem. This analysis, although valid only under unrealistic circumstances, yields insight in the problems involved in measuring phase lags. In the realistic case simulations are used to support the algorithm.

Phase lags of bright OH stars were published by Herman et al. (1985). Using observations from the same monitor program, augmented by recent observations, we use our algorithm to recalculate the phase lags published by them (Sect. 5). For some stars we get values different by more than the error assigned by Herman. Although we added data obtained since 1983 we do not claim a greater accuracy, because we believe that the errors in Herman's work are too optimistic, as they do not reflect the phase lag uncertainties from the noise on the data. We check the assumptions under which the numerical methods are valid.

Phase lags were used (Herman and Habing, 1985a, and by Diamond, 1985) to determine stellar distances. So we use the same assumptions as they did to recalculate the distances. Recent work by several authors warrants a critical look at the assumptions. Finally we discuss briefly the astronomical implications of these new distances.

"Phase lag distances" were intensively used since 1983 to study, among other things, the theory of stellar evolution (van der Veen and Habing, 1988), the processes in circumstellar shells (Heske et al., 1989; Netzer and Knapp, 1987) and the interstellar medium (Diamond et al., 1988). In addition, several new programs to measure distances to other OH/IR stars have been started recently. For instance, observations to measure the distance to the Galactic centre, by measuring the distance to several OH/IR stars close to SgrA, were started by one of us (H.J.v.L.).

All this justifies a critical look at the method of determining the phase lag from OH flux curves. Though the problems with the underlying assumptions are hard to tackle, we can improve the internal error estimate which we believe to be wrong in the original work (Herman, 1983). The new projects mentioned above are another reason for the work presented here; many of them require the reduction of multichannel spectral data.

2. The estimation problem

2.1. Assumptions

Our approach relies on two assumptions, of which the consistency can be checked internally. First we assume saturated masering, in order to assure identical flux curves in all channels of the spectral profile. Secondly we assume spherical symmetry. It is not completely clear from an astrophysical point of view that this is valid (see Sect. 6). The assumption is important, because then the phase lag changes linearily through the profile. In principle we can check both these assumptions when we deal with real data.

The observed data $g_i(t_n)$ are calibrated velocity spectra, observed at irregular time instants t_n ($n=1,\ldots,N$). The spectrum has I velocity channels v_i ($i=1,\ldots,I$), where $i=1$ and $i=I$ correspond to greatest and smallest velocity, respectively. See Fig. 2 for a typical flux curves of two stars from the Dwingeloo sample. Since we assume a saturated maser, the channels have a common flux curve $c(t)$ with individual phase lags τ_i and with individual factors u_i representing the spectral profile:

$$g_i(t_n)=u_i c(t_n-\tau_i). \tag{1}$$

Because of the assumed spherical symmetry the phase lag is a linear function of v_i,

$$\tau_i=\frac{v_i-v_1}{v_I-v_1}\tau_0, \tag{2}$$

where τ_0 is the star's overall lag, i.e. the lag between the outer channels $i=1$ and $i=I$.

In view of the large dynamic flux range it is convenient to use a log flux scale. Including the errors in log flux we get

$$f_i(t_n)=m_i+s(t_n-\tau_i)+p_i(t_n), \tag{3}$$

where $f=\log(g)$, $m=\log(u)$ and $s=\log(c)$. The $p_i(t_n)$ represent the observational errors in the log flux domain. Since the corresponding errors in the flux domain are often caused by calibration defects, with an approximately constant ratio σ_g/g, the log flux errors $p_i(t_n)$ will all be of the same order of magnitude for different t_n, but we may expect slightly different error variances between different spectral channels (see Sect. 3).

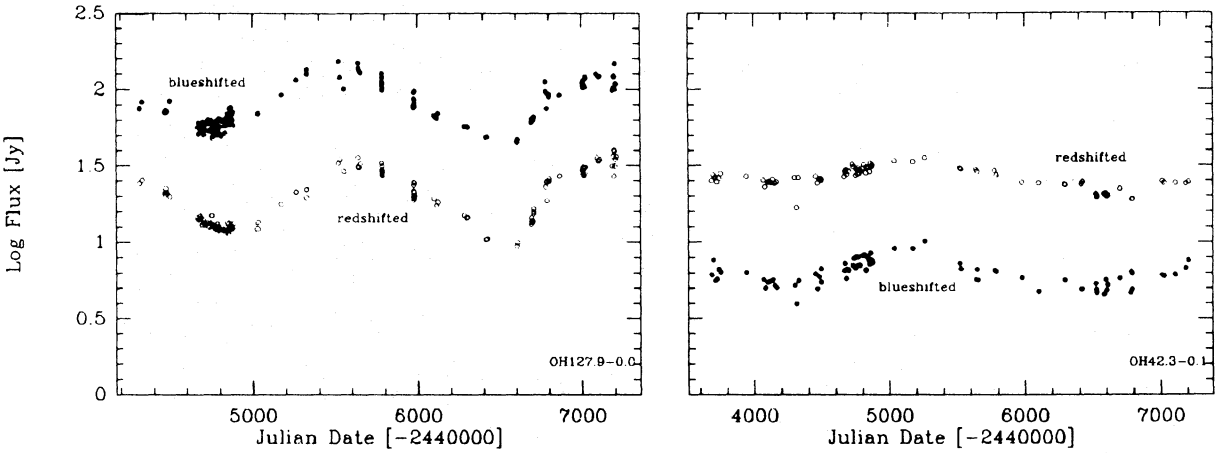

Fig. 2. Typical example of log flux curves. Shown are the variations of the outer peaks of OH 127.9+0.0 and OH 42.3−0.1, observed with the DRT

Substitution of Eq. (2) into Eq. (3) gives

$$f_i(t_n)=m_i+s\left(t_n-\frac{v_i-v_1}{v_I-v_1}\tau_0\right)+p_i(t_n), \qquad \begin{matrix} i=1,\ldots,I, \\ n=1,\ldots,N. \end{matrix} \tag{4}$$

Our problem is to produce from the data (4) an unbiased estimate $\hat{\tau}_0$ of the overall lag τ_0 and to specify its estimation error. To this end we adopt a two step procedure. First, we estimate the lags of P pairs of channels. Second, we combine the P lag estimates to obtain an estimate of the overall lag τ_0. The two steps are discussed in Sects. 2.2 and 2.3. In Sect. 2.4 we argue that $P=(I-1)$ is a sufficient number of pairs.

2.2. *Interchannel lag estimation*

Consider one channelpair, consisting of channels i and j. Their lag ("interchannel lag" or i.c. lag) follows from Eq. (2):

$$\tau_{ij}=\frac{v_i-v_j}{v_I-v_1}\tau_0\equiv x_{ij}\tau_0. \tag{5}$$

Various methods exist to obtain an estimate $\hat{\tau}_{ij}$ of τ_{ij} (e.g. Gaskell and Peterson, 1987; Edelson and Krolik, 1988). Since our arguments hold for any of these methods there is no need to define a specific one at this point. (The i.c. lag estimator we have actually used is described in Sect. 4.2). The only assumption is that we produce an unbiased estimate. Thus, if the estimate differs from the true value by an error ε_{ij},

$$\hat{\tau}_{ij}=x_{ij}\tau_0+\varepsilon_{ij}, \tag{6}$$

we require that ε_{ij} has zero mean value. Applying the i.c. lag estimation to P pairs of channels we get P equations of type (6); in vector notation

$$\hat{\boldsymbol{\tau}}=\boldsymbol{x}\tau_0+\boldsymbol{\varepsilon}, \tag{7}$$

where $\hat{\boldsymbol{\tau}}$, $\boldsymbol{x}$ and $\boldsymbol{\varepsilon}$ are column vectors of length P.

2.3. *Weighted combination*

The estimates of Eq. (7) are linearly combined with weights w_{ij} to obtain an estimate of the overall lag:

$$\hat{\tau}_0=\sum_{P\text{ pairs}} w_{ij}\hat{\tau}_{ij}=\boldsymbol{w}^{\mathrm{T}}\hat{\boldsymbol{\tau}} \tag{8}$$

where $\boldsymbol{w}$ is the (column) vector of weights, where superscript T denotes transposition and where $\boldsymbol{w}^{\mathrm{T}}\hat{\boldsymbol{\tau}}$ is the inner product of $\boldsymbol{w}$ and $\hat{\boldsymbol{\tau}}$. The weights $\boldsymbol{w}$ depend on the variances and covariances of the i.c. estimation errors ε_{ij}. If these (co)variances are known they can be represented by a $P\times P$ covariance matrix $\boldsymbol{Q}=E(\boldsymbol{\varepsilon}\cdot\boldsymbol{\varepsilon}^{\mathrm{T}})$, where $E(\ )$ denotes expectation. The weights are then given by

$$\boldsymbol{w}=\frac{1}{\boldsymbol{x}^{\mathrm{T}}\boldsymbol{Q}^{-1}\boldsymbol{x}}\boldsymbol{Q}^{-1}\boldsymbol{x}. \tag{9}$$

Equations (8) and (9) represent the minimum variance, linear, unbiased estimate of τ_0 (Kendall and Stuart, 1973). Application of (8) and (9) to (7) gives

$$\hat{\tau}_0=\tau_0+\frac{\boldsymbol{x}^{\mathrm{T}}\boldsymbol{Q}^{-1}\boldsymbol{\varepsilon}}{\boldsymbol{x}^{\mathrm{T}}\boldsymbol{Q}^{-1}\boldsymbol{x}}=\tau_0+\varepsilon_0. \tag{10}$$

Thus, the estimate $\hat{\tau}_0$ is unbiased. [$E(\varepsilon_0)=0$ since $E(\varepsilon)=0$.] Further, it is readily checked that the (minimized) error variance equals

$$\mathrm{var}(\varepsilon_0)=\frac{1}{\boldsymbol{x}^{\mathrm{T}}\boldsymbol{Q}^{-1}\boldsymbol{x}}. \tag{11}$$

2.4. *The number of interchannel lag estimates*

2.4.1. Redundant channelpairs

We shall now discuss the number of channelpairs, P, to be used in Eq. (8). The maximum number is $\frac{1}{2}I(I-1)$, but it is questionable whether I channels can produce as many as $\frac{1}{2}I(I-1)$ independent lag estimates. If some of the equations of the set (7) turn out to be linear combinations of the others, they are redundant since they provide no new information on τ_0. The effort spent in estimating their lags is superfluous. In addition, they lead to a singular matrix $\boldsymbol{Q}$, which leaves $\boldsymbol{Q}^{-1}$ undefined. Thus, redundant channelpairs must be avoided. Light is shed on this problem by deriving analytical expressions under ideal conditions for the (co)variances of the interchannel errors ε_{ij} in Eq. (7), i.e. by deriving expressions for the elements of matrix $\boldsymbol{Q}$.

2.4.2. Matrix $\boldsymbol{Q}$ under ideal conditions

The elements of $\boldsymbol{Q}$ can be calculated if we allow some simplification of the observed data [Eq. (3)]. We omit the offsets m_i and make the following assumptions.

— The observation times are equispaced, $t_n = n\Delta$, with spacing Δ small compared to the time scale of variability of the log flux curve:

$$f_i(t_n) = s(n\Delta - \tau_i) + p_i(t_n). \qquad \begin{matrix} i = 1, \ldots, I, \\ n = 1, \ldots, N. \end{matrix} \tag{12}$$

The observations span a time interval $N\Delta$.

— The errors $p_i(t_n)$ have an rms value σ_i, dependent on the spectral channel i, but independent of the observation time t_n.

— The errors $p_i(t_n)$ are uncorrelated and are small compared to the log flux curve, i.e. $\sigma_i \ll (s_{\max} - s_{\min})$.

Under these conditions we derive in Appendix A the following results for $\mathrm{var}(\varepsilon_{ij})$ (the diagonal elements of $\boldsymbol{Q}$) and for $\mathrm{covar}(\varepsilon_{ij}, \varepsilon_{kl})$ (the off diagonal elements). For the variances we get:

$$\mathrm{var}(\varepsilon_{ij}) = \alpha_i + \alpha_j, \tag{13}$$

where

$$\alpha_i = \sigma_i^2 \left(\frac{1}{\Delta} \int_0^{N\Delta} (\dot{s}(t))^2 \, \mathrm{d}t \right)^{-1}. \tag{14}$$

Expressions (13) and (14) are intuitively satisfying. The i.c. lag error decreases when σ_i decreases and when the number of observations increases. Flux curves with steep ascents and/or descents [large values of $\dot{s}(t)$] perform better than curves with gradual slopes. Equations (13) and (14) can be rewritten as a simple rule of thumb for the accuracy of a two channel lag estimate (Sect. 3.1). Equation (13) is a special case of

$$\mathrm{covar}(\varepsilon_{ij}\varepsilon_{kl}) = \delta_{ik}\alpha_i + \delta_{jl}\alpha_j - \delta_{il}\alpha_i - \delta_{jk}\alpha_j, \tag{15}$$

where

$\delta_{ij} = 1$ when $i = j$, $\quad \delta_{ij} = 0$ when $i \neq j$.

Expression (15) implies that the i.c. lag errors are indeed correlated in a way that makes many of the maximum number of $\frac{1}{2}I(I-1)$ lag estimates redundant. It can be shown from (15) that matrix $\boldsymbol{Q}$ is of rank $(I-1)$. Thus we find – not surprisingly – that the I spectral channels provide a maximum of $(I-1)$ independent measurements that can be used to estimate $\hat{\tau}_0$. The situation can be explained in terms of closure errors. Suppose, for example, that we estimate the lags between 3 channels i, j and k. The true lag values satisfy by their definition (5) the relation $\tau_{ik} - \tau_{ij} - \tau_{jk} = 0$. A similar relation, however, turns out to hold for their estimates: $\hat{\tau}_{ik} - \hat{\tau}_{ij} - \hat{\tau}_{jk} = 0$. This follows from Eq. (15) by showing that the closure error has zero variance:

$$\mathrm{var}(\varepsilon_{\mathrm{clos}}) \equiv \mathrm{var}(\varepsilon_{ik} - \varepsilon_{ij} - \varepsilon_{jk}) = 0. \tag{16}$$

Hence only two of the three estimates $\hat{\tau}_{ik}$, $\hat{\tau}_{ij}$ and $\hat{\tau}_{jk}$ are non-redundant.

2.4.3. Selection of $(I-1)$ channelpairs

As shown above we may (and must) limit the number of inter-channel lag estimates to $P = (I-1)$. One can prove that it does not matter which of the I channels are used to form pairs, provided that every channel is used at least once. We shall proceed, somewhat arbitrarily, by selecting one channel as a reference channel [we take the channel with maximum value u_i in Eq. (1)] and by forming $(I-1)$ pairs between the reference channel and each of the others.

2.5. Explicit expressions

We return briefly to the algorithm of Sects. 2.2 and 2.3. Expression (7) is now a set of $(I-1)$ equations, and can be rewritten as

$$\hat{\tau}_{ri} = x_{ri}\tau_0 + \varepsilon_{ri}, \qquad i = 1, \ldots, I, \; i \neq r \tag{17}$$

where r indicates the reference channel. The estimates must be weighted in the manner of Eq. (8), which requires computation of the weights $\boldsymbol{w}$, which in turn requires inversion of an $(I-1) \times (I-1)$ covariance matrix $\boldsymbol{Q}$ (Eq. 9). Under the ideal conditions (12) the elements of $\boldsymbol{Q}$ are given by Eqs. (13) and (14) and it appears that $\boldsymbol{Q}$ can be inverted algebraically. As a result, we derive in Appendix B the following explicit expressions for the estimate of the overall lag and for its error variance:

$$\hat{\tau}_0 = \frac{U_{x\tau} - U_x U_\tau / U}{U_{xx} - U_x^2 / U} \tag{18}$$

$$\mathrm{var}(\varepsilon_0) = \frac{1}{U_{xx} - U_x^2/U}, \tag{19}$$

where

$$U = \sum_{i=1}^{I} \frac{1}{\alpha_i},$$

$$U_x = \sum_{\substack{i=1 \\ i \neq r}}^{I} \frac{x_{ri}}{\alpha_i}, \quad U_{xx} = \sum_{\substack{i=1 \\ i \neq r}}^{I} \frac{x_{ri}^2}{\alpha_i},$$

$$U_\tau = \sum_{\substack{i=1 \\ i \neq r}}^{I} \frac{\tau_{ri}}{\alpha_i}, \quad U_{x\tau} = \sum_{\substack{i=1 \\ i \neq r}}^{I} \frac{x_{ri}\tau_{ri}}{\alpha_i}. \tag{20}$$

2.6. Implementation by simulation

Sections 2.4.2, 2.4.3 and 2.5 are valid only under the simplifying restrictions (12), which are not satisfied by our observational data. For example, Eq. (14) looses its quantitative significance when the conditions are unfulfilled and cannot be used to compute the various quantities U that are required in the expressions for $\hat{\tau}_0$ and $\mathrm{var}(\varepsilon_0)$ [Eqs. (18) and (19)].

On the other hand, it is reasonable (and practical!) to assume that the number of independent channel pairs remains $(I-1)$ under realistic conditions, and that we can use Eqs. (18), (19) and (20) to solve the problem. We have adopted this approach in the practical implementation of our algorithm (Sect. 4). At most, should our assumption fail, we produce an estimate $\hat{\tau}_0$ with a somewhat larger than minimum error, but the estimate remains unbiased [Eq. (10)].

This leaves us with the problem to determine the values of α_i. The problem is solved by simulation. We generate a large number ($M \approx 100$) of artificial datasets using the original observation times t_n and using a log flux curve $s(t)$ and a preliminary estimate $(\hat{\tau}_0)_{\mathrm{prelim}}$ derived from the observed data. Artificial errors $p_i(t_i)$, statistically equivalent to those in the actual observation, are added to mimic the observed data. From the M sets we estimate the left hand side of Eq. (13) and we calculate the values of

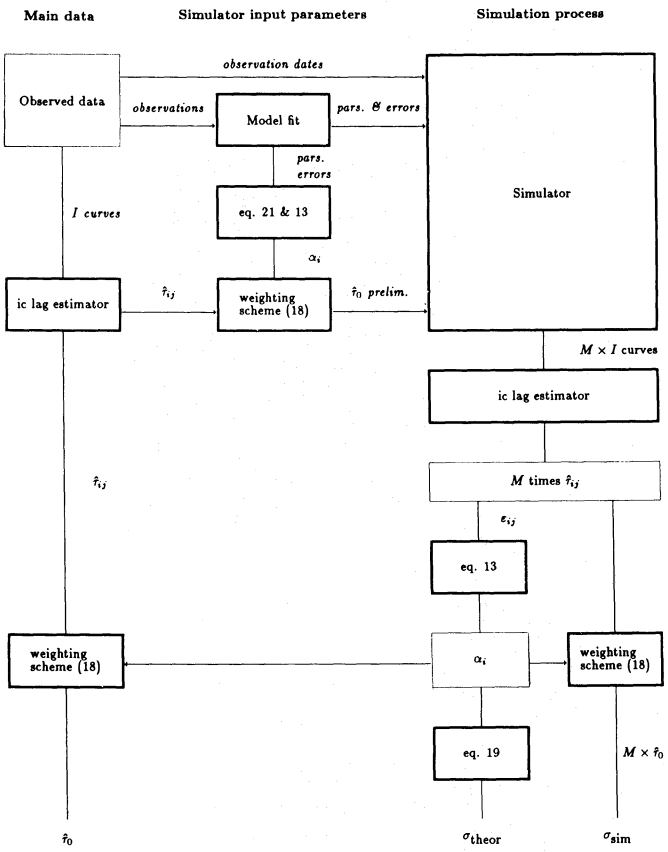

Fig. 3. Block diagram of the data reduction

$\alpha_1, \ldots, \alpha_I$. A block diagram of these steps is presented in Fig. 3.

The $\alpha_1, \ldots, \alpha_I$ are then used in Eq. (20), together with $\hat{\tau}_{ri}$ of the observed data, to obtain the quantities U required for the final estimate $\hat{\tau}_0$ (Eq. 18). See the block diagram. They are similarly applied to the M sets of simulated $\hat{\tau}_{ri}$ to procedure M simulated estimates of τ_0. The variance of this set, $\mathrm{var}(\varepsilon_0)_{\mathrm{sim}}$, is the error variance of our estimate.

Finally, the $\alpha_1, \ldots, \alpha_I$ are substituted into Eq. (19) to give a second error variance, $\mathrm{var}(\varepsilon_0)_{\mathrm{theor}}$, representing the error expected under the ideal conditions (12). A ratio $\mathrm{var}(\varepsilon_0)_{\mathrm{sim}}/\mathrm{var}(\varepsilon_0)_{\mathrm{theor}}$ significantly greater than 1 indicates a deviation from ideal conditions.

The approach by simulation removes the need to make simplifying assumptions concerning the observed data or concerning the i.c. lag estimator. Departures from ideal conditions are automatically taken care of by the simulation.

3. Some considerations for monitor programs

3.1. Extending the analytical approximations

Before we discuss the implementation of the algorithm we derive some rules of thumb for monitoring programs.

Expressions (13) and (14) give the error on the estimate of the lag between two channels. This result was derived under several assumptions (Sect. 2.4.2). Under more realistic conditions we can use the formulas to derive a lower limit to the error. A numerical value can be obtained by assuming a specific form for $s(t)$ and evaluating expression (14).

We choose for the log flux variability $s(t)=b\cos(2\pi(t-t_0)/P)$. When the observation period $N\Delta$ is larger than the period P we derive

$$\mathrm{var}(\varepsilon_{ij}) \approx \frac{1}{2\pi^2}\left(\frac{1}{N}\frac{\sigma_i^2+\sigma_j^2}{b^2}\right)P^2. \tag{21}$$

The errors in the log flux can be replaced by corresponding errors in the flux, giving

$$\mathrm{var}(\varepsilon_{ij}) \approx \frac{1}{2\pi^2 \ln(10)}\left(\frac{1}{N}\frac{(\sigma_g/g)_i^2+(\sigma_g/g)_j^2}{b^2}\right)P^2 \tag{22}$$

where (σ_g/g) is the relative error in a flux measurement and b is again the amplitude of the log flux curve.

3.2. The limits set by calibration

It is generally not true that the factors (σ_g/g) are determined by the noise in the individual spectra. The values reflect, through Eq. (21), the relative accuracy with which we can follow the variations. So the (σ_g/g) can be limited to an approximately constant ratio, because the calibration is performed with limited accuracy. This turns out to be often the case and justifies our choice to work with the log flux curve (Sect. 2.1).

The calibration defect can have its origin in the total flux calibration. This may introduce a bias. If the whole spectrum is scaled wrongly, different parts of the spectrum become correlated. This way the phase lags $\hat{\tau}_{ij}$, and thus $\hat{\tau}_0$, will become biased towards zero. Therefore this bias would yield phase lags too small and stellar distances too small. In the case a whole sample of stars is monitored with a single telescope, doing a selfcalibration of the whole dataset may be a way to cure this (Herman and Habing, 1985b).

Most often the cross band calibration will limit the accuracy of the flux measurements. When baseline subtraction is necessary some channels may become correlated while others get anticorrelated. We may hope that this will not bias the final answer, but it will limit the relative accuracy for many single dish monitor programs.

Taking the calibration limits into consideration we can estimate the error on $\hat{\tau}_{ij}$ for a particular set of observations. By using more than one pair of channels we can improve our estimate of the diameter of the shell. This improvement will be modest, but important. For OH/IR stars the inner channels are less sensitive to the phase lag and usually have less signal. Evaluating expressions (19) and (20) for a typical OH spectrum with a channel separation of 1 km s^{-1}, we find that the final standard deviation of $\hat{\tau}_0$ is a factor of 2 smaller than that on $\hat{\tau}_{ij}$ of the outer two channels.

4. Implementation

4.1. Block diagram

Figure 3 illustrates the procedure as implemented for the Dwingeloo OH/IR data. The diagram consists of 3 parts.

Main data stream. The main stream consists of $(I-1)$ interchannel lag estimates, followed by a weighted combination to give the desired estimate $\hat{\tau}_0$ of the observed star. The interchannel lag estimator is described separately in Sect. 4.2. The weighted

combination uses Eqs. (18) and (20) (instead of the original Eq. 8) and requires its weights in the form of quantities $\alpha_1, \ldots, \alpha_I$.

Simulation process. The quantities $\alpha_1, \ldots, \alpha_I$ are obtained from a variance analysis of M (≈ 100) sets of simulated data, as described in Sect. 2.6. The simulation also provides the variance of the estimation error, $\mathrm{var}(\varepsilon_0)_{\mathrm{sim}}$. A second error variance, $\mathrm{var}(\varepsilon_0)_{\mathrm{theor}}$, is produced for diagnostic use (Sect. 2.6). The error variances are converted to rms errors, σ_{sim} and σ_{theor}, respectively.

Simulator input parameters. In order to get a realistic simulation of the observed data we must know a number of parameters: (i) the underlying log flux curve $s(t)$ of the observed star (Sect. 2.1), (ii) the statistics of the observational errors $p_i(t_n)$ (Sect. 2.1), (iii) a preliminary estimate of the star's overall lag τ_0. The computation of these input parameters is briefly described in Sect. 4.3.

4.2. The interchannel lag estimator

Consider the log flux data in two spectral channels i and j. From Eq. (3):

$$f_i(t_n)=m_i+s(t_n-\tau_i)+p_i(t_n)$$
$$f_j(t_n)=m_j+s(t_n-\tau_j)+p_j(t_n). \tag{23}$$

The curves $s(t)$ have a more or less periodic character and the observations usually span a time interval larger than one period. The sample raster t_n is irregularly spaced, but the average sample distance is fairly small, i.e. 1/20 of a period.

We require an unbiased estimate of the interchannel lag $\tau_{ij}=\tau_j-\tau_i$. Various algorithms can be designed to try and achieve this goal. We have selected a method consisting of the following four steps.

Linear interpolation. The discrete data (23) are made continuous by linear interpolation: adjacent values $f(t_n)$ and $f(t_{n+1})$ are joined by straight lines. The resulting curves, consisting of straight line segments, are resampled equidistantly with a sampling distance d, small compared to the expected interchannel lag τ_{ij}.

Offset removal. The offsets m_i and m_j are estimated by averaging and are removed by subtraction. The resulting data are $f_i'(nd)$ and $f_j'(nd)$.

Lag estimation. The lag is estimated by shifting one curve with respect to the other and by searching for the shift l that minimizes the sum of squared differences,

$$R_l=(n_2-n_1+1)^{-1}\sum_{n=n_1}^{n_2}(f_i'(nd)-f_j'((n-l)d))^2. \tag{24}$$

The initial estimate $\hat{\tau}_{ij}$ is given by $\hat{l}d$, where $\hat{l}$ is the shift that minimizes expression (24) (n_1 and n_2 delimit the common interval of overlap, taking account of the shift l).

Bias removal. The initial estimate may be biased when the observation times t_n are badly positioned with respect to the log flux curve, or when large gaps $t_{n+1}-t_n$ occur. We calculate the bias by repeating the previous three steps for noisefree observations, based on the log flux curve and the preliminary estimate $(\hat{\tau}_0)_{\mathrm{prelim}}$, prepared as input to the simulator (Fig. 3). A plot of $\hat{l}d$ versus the true value τ_{ij} is then used to correct for the bias.

4.3. Simulation parameters

The weighted combination of i.c. lag estimates requires weights $\alpha_1, \ldots, \alpha_I$ that are obtained from M simulations of the observed data. So the simulator must be provided with a log flux curve, with the statistics of $p_i(t_n)$ and with a preliminary estimate of the overall phase lag τ_0. In addition we must provide the set of observation times, t_n, to the simulator. See Sect. 2.6 and Fig. 3.

The log flux curve is obtained by fitting the following model to the observed data

$$s(t)=b\cos(2\pi\phi(t)), \tag{25}$$

where

$$\phi(t)=\begin{cases}\dfrac{\varphi}{2f} & \text{when } 0\le\varphi<f,\\[2ex] \dfrac{\varphi-1}{2(1-f)}+1 & \text{when } f\le\varphi\le 1,\end{cases}$$

and

$$\varphi=(t-t_0)/P.$$

P is the period, t_0 is the phase, b is the amplitude and f is the asymmetry parameter which equals the risetime over the total period and thus has a value between 0 and 1. We have used a nonlinear least squares method for the fitting. Because P and f are not strictly independent we fitted first with a fixed f, then with a fixed P and switched back and forth in this way before reaching the final result. Further we have used the fact that b, P, f and – in first approximation – t_0 are identical for all channels if the maser is saturated.

The error variances $\sigma_i(t_n)$ were measured from the residuals of the fit from those sections of the observed data where a good fit was possible. We usually could not use the whole curve to determine the noise statistics, because systematic departures from the model were present. It is a known fact that the variations from Long Period Variables show irregularities. This also implies that our model does not describe the data extremely accurate, but this will only have a small influence on the variance in the final estimate of τ_0, but will not introduce any bias.

Finally, a preliminary estimate of τ_0 was obtained by using Eqs. (18) and (21).

5. Dwingeloo monitor

5.1. Introduction

We now apply the method to data obtained with the Dwingeloo Radio Telescope (DRT). The sample under consideration is defined in Herman and Habing (1985b). It consists of 60 bright OH sources with double peaked spectra ($S_{1612}>4$ Jy) at low Galactic latitudes and also some Mira's and Supergiants.

Approximately 100 times the 1612 MHz profile for each star was observed over a period of 10 years. Unfortunately data were only recorded for discrete peaks in the spectra (typically 6 peaks per spectrum), so that we have information from only a small number of channels.

Calibration of the observations was done against a noise tube that was calibrated daily during observations against Virgo A. Also a daily reference measurement of an empty sky was made. The observed spectra needed baseline fitting before flux measurements could be made. This was sometimes difficult when the OH spectrum already filled a large fraction of the good quality part of the pass-band. In some cases the data also suffered from confusion (see Herman and Habing, 1985b, for details).

Table 1. Parameters of the log flux curves of our sample

Name	10^m (Jy)	P (d)	σ_P	b	σ_b	t_0 (JUL-2440000)	σ_{t_0}	f	σ_f
R Aql	4.1	282	21	0.2453	0.0176	5200.5	10.1	0.612	0.038
RR Aql	7.9	386	28	0.1369	0.0104	4936.1	22.3	0.246	0.032
SY Aql	1.4	349	26	0.1100	0.0066	5198.5	19.2	0.529	0.059
VY Cma	No fit possible								
PZ Cas	Not variable; <0.108								
NLM Cyg	349.6	1469	351	0.0353	0.0062	4576.4	258.4	0.262	0.085
Z Cyg	3.9	261	17	0.1286	0.0085	5157.2	12.1	0.331	0.036
U Ori	No fit possible								
WX Psc	35.3	634	23	0.2076	0.0065	4991.2	18.3	0.354	0.021
WX Ser	2.0	413	34	0.1531	0.0119	5200.2	20.3	0.477	0.057
IK Tau	4.4	461	16	0.3316	0.0101	5088.4	8.8	0.438	0.018
RS Vir	6.2	355	15	0.1630	0.0062	5064.0	11.7	0.234	0.024
359.4−1.3	4.4	2835	282	0.1454	0.0168	4422.4	279.1	0.145	0.134
0.3−0.2	No fit possible								
1.5−0.0	No fit possible								
11.5+0.1	17.8	826	131	0.0271	0.0038	5114.0	83.7	0.419	0.082
12.3−0.2	6.7	584	78	0.1320	0.0165	5114.2	43.4	0.507	0.075
12.8−1.9	12.0	1024	111	0.2282	0.0269	4929.3	74.6	0.309	0.040
12.9+0.9	3.9	1522	142	0.0941	0.0072	4801.1	35.2	0.852	0.051
13.1+5.0	13.3	698	65	0.0950	0.0074	4883.2	40.6	0.580	0.078
15.7+0.8	No fit possible								
16.1−0.3	18.7	2271	132	0.1326	0.0075	5112.8	95.2	0.428	0.034
17.4−0.3	9.1	1667	144	0.2112	0.0142	3914.9	105.9	0.222	0.035
17.7−2.0	No fit possible								
18.3+0.4	7.5	782	113	0.0734	0.0107	5134.8	62.0	0.619	0.119
18.5+1.4	No fit possible								
18.8+0.3	Not variable; <0.043								
20.2−0.1	7.8	811	170	0.1458	0.0257	5194.6	99.3	0.489	0.098
20.7+0.1	12.6	1672	98	0.1619	0.0084	4841.7	88.0	0.214	0.036
21.5+0.5	23.1	1785	114	0.2094	0.0119	3935.7	65.4	0.358	0.032
25.1−0.3	Not variable; <0.052								
26.2−0.6	18.2	1172	94	0.1386	0.0106	4656.1	61.3	0.458	0.063
26.4−1.9	16.9	566	55	0.0991	0.0078	4712.4	29.4	0.517	0.066
26.5+0.6	56.1	1589	42	0.2272	0.0046	4764.2	28.9	0.313	0.023
27.3+0.2	32.5	830	59	0.1272	0.0082	4675.6	49.2	0.215	0.042
28.5−0.0	10.2	621	62	0.1364	0.0120	5005.2	40.0	0.490	0.051
28.7−0.6	12.0	669	32	0.1736	0.0069	4768.1	20.5	0.484	0.032
30.1−0.2	12.9	960	48	0.1583	0.0088	5414.4	31.4	0.409	0.040
30.1−0.7	57.6	2013	243	0.0921	0.0113	5301.9	155.0	0.366	0.045
30.7+0.4	Confusion								
31.0−0.2	No fit possible								
31.0+0.0	No fit possible								
32.0−0.5	10.3	1417	108	0.1695	0.0124	5001.0	84.0	0.402	0.060
32.8−0.3	27.8	1539	31	0.2473	0.0042	4706.2	24.0	0.410	0.017
35.6−0.3	20.1	840	42	0.1554	0.0072	5151.9	29.7	0.346	0.032
36.9+1.3	4.1	425	35	0.1292	0.0103	5081.2	24.7	0.387	0.056
37.1−0.8	No fit possible								
39.7+1.5	73.6	1430	27	0.1606	0.0027	4808.8	19.9	0.406	0.014
39.9−0.0	8.5	778	87	0.1324	0.0132	5192.4	69.0	0.404	0.084
42.3−0.1	6.6	2344	445	0.1013	0.0199	4970.7	348.2	0.249	0.065
44.8−2.3	21.0	534	24	0.1600	0.0065	5072.3	16.7	0.393	0.030
45.5+0.1	8.7	697	31	0.1705	0.0070	5001.5	21.9	0.458	0.029
51.8−0.2	No fit possible								
53.6−0.2	No fit possible								
75.3−1.8	6.5	1652	48	0.2884	0.0077	4439.2	34.0	0.302	0.023

(*continued*)

Table 1 (continued)

Name	10^m (Jy)	P (d)	σ_P	b	σ_b	t_0 (JUL-2440000)	σ_{t_0}	f	σ_f
77.9+0.2	No fit possible								
83.4−0.9	12.9	1188	148	0.2014	0.0195	5008.7	114.6	0.407	0.044
104.9+2.4	36.6	1460	24	0.2155	0.0028	4862.1	20.5	0.400	0.013
127.9−0.0	83.7	1638	57	0.1901	0.0063	5558.3	38.2	0.439	0.026
138.0+7.2	20.4	1276	150	0.1990	0.0267	5362.5	86.1	0.384	0.040

The program started in 1978 and has continued into 1988. Herman's analysis was based on data from the period 1978–1983. However, in the period 1983–1988 data were obtained less frequently and were of lower quality. This was partly due to frequent interference at 1612 MHz by the GLONASS sattelites (Carter, 1986). Therefore the bulk of the data used in our present analysis is identical to the data used by Herman.

5.2. *Flux curves*

First the velocity tracking over the years was checked. We had to be sure all spectra are lined up. This turned out to be no problem for the DRT.

We continued with fitting the asymmetric cosine models (25) to our log flux curves for $f(t)$. The fits were made with the procedure described in Sect. 4.3. In almost all cases (except for VY CMa) different channels in the spectrum could be fitted with the same log flux curve, and with the same value for b. This justifies our assumption of saturated masering, which we have made throughout this paper.

Most often the deviations from the fitted model were greater than expected from the thermal noise in the spectrum. From the log flux curves it was clear that this was not due to a wrong model, so we conclude that the deviations are caused by calibration defects. We checked the residuals of all observations on a daily basis for systematic effects. We are convinced that the quality of the log flux curves is mainly affected by bandpass calibration for these bright sources.

In Table 1 we present the parameters that describe the log flux curve. Because some stars have many spectral channels we list in column 2 the value of 10^{m_i} [Eq. (3)] belonging to the brightest channel. Note that some periods we found are larger than 2000 d: such values could not be measured by Herman in his monitor program. We have estimated the errors on the parameters of our model from the goodness of the fit.

In Fig. 4 we plot the measured signal to noise obtained from the model fit against expected signal to noise ratio from thermal noise. The maximum value of ≈ 20 is due to a limit of 5% in cross-band calibration. Using formula (22) we can see that we get errors on the phase lag for a typical OH/IR star ($P=1000$ d, $b=0.1$) in the order of 10 d, i.e. 30% of the total lag. So it is quite difficult to get very accurate phase lags for ordinary OH/IR stars with these data. Good results are obtained only for stars that vary with large amplitudes. These are not necessarily the bright stars in our sample. We hope that a new correlator with 1024 channels will improve our results in the future by making a better bandpass calibration possible.

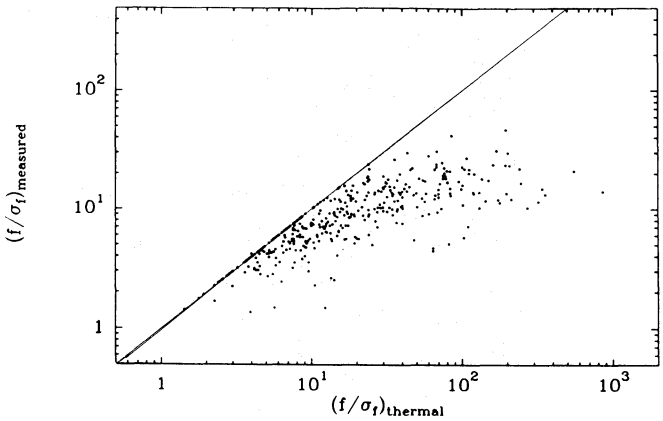

Fig. 4. Expected dynamic range versus measured relative errors. Clearly the calibration is limited to 5%

5.3. *Resulting phase lags; checking the assumptions*

The results of our calculations are shown in Table 2.

First we check our basic assumptions (see Sect. 2.1). We have already seen, in Sect. 5.2, that all but one stars have variations consistent with saturated masering. We have also checked for any systematic departure from linearily increasing phase lags across the profile. No such effect was found within the errors. This is not very conclusive on the issue of spherical symmetry, because individual lags usually have large errors, but it does validate our method; in particular the use of Eq. (2).

We show $(\sigma^2_{sim}/\sigma^2_{theor})$ in the fourth column. If $\boldsymbol{Q}$ has the special structure we described in Sect. 2 this value must be 1. In 67% of 43 cases the simulated error was within 10% of the theoretically predicted error. The differences are partly explained by the limited size of each simulation. This result justifies our assumption that we can use the special form of $\boldsymbol{Q}$ of size $(I-1)$. Serious differences were found for the cases where either the data were of poor signal to noise or where large time gaps occured in the observations. In the latter case we also found substantial bias in the i.c. lag estimate. The bias was removed by the method explained in Sect. 4.2.

A minimum check of our method and the underlying assumptions is that all phase lag estimates must have a positive value. Indeed this is observed within the uncertainties.

We compared our results with those found by Herman. In general we found that the differences between both values are reasonably small. In a more formal comparison we estimated the

error in Herman's determinations (Herman and Habing, 1985b) and tested whether the two values of the phaselags are statistically the same. We have found that there is a small, but significant difference. A check revealed that this is due to differences in the algorithm used. We favour the new values, because a formally more correct weighting scheme was used to get to the final value of $\hat{t}_0$. Especially the values for OH 127.9−0.0, OH 32.8−0.3 and OH 75.3−1.8 differ from the phase lag calculated by Herman.

6. Phase lags and distances

6.1. Underlying assumptions

The values found can now be used to calculate new values for "phase lag" distances of our stars.

When measuring the phase lag we assume the shell to be unresolved to our telescope and we discriminate between emission from different parts of the shell by the Doppler shift. As mentioned before some of the shells can be resolved with synthesis telescopes. The cones will then show as compact regions and the weak emission, at velocities near the stellar velocity (i.e. halfway between the two peaks), is seen as a ring. We can then determine the angular diameter of the shell. Combining the phase lag and a measurement of the angular size of the shells would then give the stellar distance, according to the simple model.

To get a *correct* distance the emission from which we measure the phase lag must originate at the same distance from the star as the emission we use to determine the angular diameter. The phase lag measurement is dominated by the outer parts of the spectral profile, while the angular size is obtained from radiation from the inner part of the spectrum. Hence we must rely on two assumptions:

Spherical symmetry. Several interferometric observations support this assumption, although for a few stars severe deviations have been reported. The blobbiness observed in these sources indicates departures from our simple model. One should be aware, however, that interferometric observations and the techniques to analyze them emphasize the blobbiness. The maps of the stars in our sample with the VLA often indicate that the assumption of spherical symmetry is rather well justified.

Emission in different directions from the same parts of the shell. Because maser shells emit non-isotropically (Alcock and Ross, 1986), a systematic error in distance is possible even with a spherically symmetry shell. Theoretical calculations show that the emission perpendicular to the outflow velocity can originate closer to the star than the emission that is emitted along the velocity axis. The emission along the velocity axis forms the blue- and redshifted peaks, which contain most of the information for the determination of the phase lag, while the ring consists of radiation that is emitted perpendicular to the outflow velocity. This effect could thus result in measuring distances that are too large. It turns out to be very difficult to estimate the magnitude of this bias.

If the maser shells are thin this effect decreases. Although the thin shell model is valuable to explain the overall shape of the spectral profiles (Cohen, 1989), recent theoretical work indicates that OH molecules are present over a large range in radii (Nertzer and Knapp, 1987). Because of the non-isotropic nature of the emission, this is not in contradiction with the measured thickness of the shell from maps (Herman et al., 1985). Theoretical estimates of this bias are possible in principle. One reason to assume this bias to be small is given by the realisation that the shell thickness is not large compared to the coherent pathlength of the maser. Anyway, we are left with an assumption for which no quantitative check exists. The only possible (observational) check of this assumption lies in measured distances themselves. We can try to measure the distance to several OH/IR stars at the same distance (e.g. Galactic centre) and so reveal a bias.

Table 2. Phase lags found for those stars that are clearly variable. (The last column justifies our assumption concerning Q

Name	τ_0 (d)	σ_{sim}	$\left(\frac{\sigma_{sim}}{\sigma_{theor}}\right)^2$
R Aql	0.7	2.5	0.88
RR Aql	−3.6	3.9	1.19
SY Aql	164.2	90.6	1.05
NLM Cyg	−2.9	55.7	1.56
Z Cyg	2.5	5.9	0.99
WX Psc	34.0	5.6	0.95
WX Ser	33.9	7.0	0.90
IK Tau	9.7	2.4	0.98
RS Vir	−1.9	3.8	1.12
32.8−0.3	79.5	3.5	0.83
359.4−1.3	−26.6	108.9	1.46
11.5+0.1	−11.1	77.4	1.32
12.3−0.2	−145.1	198.4	1.01
12.8−1.9	1.7	7.9	1.11
12.9+0.9	35.3	59.7	1.38
13.1+5.0	24.0	18.2	1.17
16.1−0.3	38.3	34.5	1.50
17.4−0.3	49.6	16.1	1.07
18.3+0.4	−8.1	143.9	1.24
20.2−0.1	15.9	119.1	1.34
20.7+0.1	48.4	13.0	1.26
21.5+0.5	92.4	15.2	1.24
26.2−0.6	39.3	17.3	1.11
26.4−1.9	1.0	11.1	0.93
26.5+0.6	37.4	6.9	0.92
27.3+0.2	22.2	14.3	1.00
28.5−0.0	−5.8	9.8	0.85
28.7−0.6	13.9	4.7	1.11
30.1−0.2	8.3	9.6	0.98
30.1−0.7	3.6	13.7	0.97
32.0−0.5	73.2	12.0	1.12
35.6−0.3	19.6	7.8	1.19
36.9+1.3	12.5	7.3	0.67
39.7+1.5	22.6	5.5	0.98
39.9−0.0	20.2	13.1	1.22
42.3−0.1	52.6	24.0	1.11
44.8−2.3	17.0	5.1	1.28
45.5+0.1	30.3	4.5	0.71
75.3−1.8	42.5	10.8	0.94
83.4−0.9	−10.6	21.0	0.96
104.9+2.4	32.6	5.5	1.34
127.9−0.0	41.4	8.4	0.91
138.0+7.2	0.5	20.9	0.94

If we do make the two assumptions we may continue with the straightforward formula

$$R=\frac{1}{2}\tau_0 c, \tag{26}$$

to calculate the radius of the circumstellar shell. For those stars where an angular size was known the distance was calculated, provided a significant measurement of the phase lag was obtained ($\tau_0 > 2\sigma_\tau$). The values are given in Table 3. In some cases different authors give measurements for the same angular sizes; we list the distances obtained with these values separately. The error in the distance is calculated from both the uncertainties in phase lag and angular size, but usually this value is dominated by the error in the phaselag.

These distances differ from the results by Herman and Habing (1985a), because of the different phase lags; substantially different distances are found for OH 127.9−0.0 and OH 32.8 −0.3, two stars for which the previous distance estimate gave problems.

We have used the distances to determine bolometric luminosities. Following the method of Van der Veen and Breukers (1989) we have used IRAS 12 and 25 μm fluxes to calculate the total luminosity of these stars. Because the stars are variable we have used IRAS Working Survey Data Base (WSDB) fluxes and corrected for variability using expression (25) and the values from Table 1. We thus assumed that our log flux model describes the variations of the bolometric magnitude as well as those of the 18 cm radiation. This is reasonable because the IR, where the star emits most of its energy, pumps the maser. The value of b (and maybe f) may be slightly different, because the pump is believed to operate at slightly longer wavelengths. Where the data allowed us, we have made an estimate of b_{IR} for this purpose. We present the calculated luminosities in Table 3 as well. Note that these values do not include the effects of interstellar extinction. This may affect the luminosity by a factor of two for the stars at large distances.

Table 3. Distances and luminosities of stars for which an accurate phase lag was determined and for which a measurement of the angular size was available. References are: 1. Herman et al. (1985), 2. Herman and Habing (1985), 3. Baud (1981), 4. Chapman et al. (1984), 5. Diamond et al. (1985), 6. Chapman (1985), 7. Steeman et al. (1989)

Name	D (kpc)	σ_D	L ($10^3\,L_\odot$)	σ_L	Ref.
WX PSC	0.74	0.15	39.4	16.0	3
20.7+0.1	5.06	1.38	5.9	3.2	1
21.5+0.5	8.51	1.41	96.9	32.1	1
21.5+0.5	7.34	1.38	72.1	27.1	6
26.5+0.6	1.44	0.27	21.6	8.1	1
26.5+0.6	1.30	0.35	17.6	9.5	5
28.7−0.6	1.45	0.49	6.1	4.1	7
32.0−0.5	11.87	2.70	67.2	30.6	1
32.8−0.3	5.02	0.25	23.1	2.3	1
35.6−0.3	4.21	1.70	5.8	4.7	7
39.7+1.5	2.04	0.50	36.3	17.8	2
39.7+1.5	0.98	0.34	8.4	5.8	5
44.8−2.3	1.13	0.34	4.3	2.6	2
104.9+2.4	2.30	0.40	11.7	4.1	2
127.9−0.0	2.90	0.60	56.8	23.5	2

Disregarding this, we find that most luminosities are well below the so called AGB-limit. This limit is a result from stellar evolution theory. If these OH/IR stars are the progenitors of planetary nebulae and eventually become white dwarfs, then the core mass of the star should not exceed the Chandrasekhar limit. The core mass, on the other hand, yields an upper limit for the luminosity at this mass through a relation between core mass and luminosity (Paczinsky, 1971). This gives a limit of 59 000 $L_\odot$. We thus argue that the observed luminosities are not in contradiction with a model in which these stars are eventually evolving into planetary nebulae and white dwarfs.

But even although our stars are below the AGB-limit, they are still very luminous compared to infrared selected AGB objects of which the luminosities are derived statistically (Habing, 1987; van der Veen and Habing, 1988), for which typically 5000 $L_\odot$ is found. We have discussed the possibility of a bias in the phase lag method (Sect. 6.1) and one through calibration errors (Sect. 3.2) of which the first puts these stars too far away, but we are convinced this effect is smaller than the typical errors on our distances. We thus find that the stars selected for monitoring are of high luminosity.

There are three possible selection effects which could account for this. First and most obvious is that by selecting bright OH sources we select bright IR sources. Though the relation between IR and OH is not well established, nor very narrow (Röttgering, 1989), some general relation should be present which could account for this (Herman et al., 1984). Another possibility is that we have made a selection effect, because we can only determine accurate distances to stars that are highly variable. Perhaps through evolutionary effects these are the brightest objects. Third these stars were all selected to lie within the plane of the Galaxy. This way we definitely will bias the sample in favour of the more massive AGB stars with the higher luminosities (Likkel, 1989).

7. Conclusions

We have derived an algorithm to measure phase lags from series of OH spectra. In this algorithm we can use all channels available in the spectrum. It is based on combining phase lags $\hat{\tau}_{ij}$ measured between pairs of channels. The statistical weights for the combination are obtained from simulations. This also determines the error in the final answer. Under simplifying assumptions we show that there are $(I-1)$ independent pairs in an I channel spectrum. This yields a simple algebraic scheme to combine the individual $\hat{\tau}_{ij}$. We show that it is justifiable to apply the algorithm to real data, despite the assumptions made.

We derive, under further assumptions, an expression for the error in phase lags in terms of observational parameters. We can thus predict the accuracy with which a phase lag can be obtained. This is important for new monitor programs.

Single dish experiments to measure these lags are usually limited by calibration shortcomings. Miscalibration of the total flux scale during observations can introduce a bias in the final result. We have argued that the deviations on short time scales from smooth flux curves on DRT data are caused by cross-band calibration effects. The suggestion by Herman and Habing (1985b) that these deviations reflect the thickness of the shell seems superfluous.

More accurate phase lags from single dish telescopes can be obtained by long and careful monitoring of strongly varying OH/IR stars. Instrumental improvements to the situation described for this project are possible. For instance, more correlator channels improve the situation, because of better cross-band calibration. Especially the use of synthesis telescopes for monitoring is advantageous. For instance, simulations as well as analytic calculations, show that even with a limited number (25) of observations accurate phase lags can be obtained for OH/IR stars at the Galactic Centre using the VLA. This is mainly so because we have a stable cross-band calibration and the possibility to resolve out the background radiation. We believe phase lags can be measured with 10% accuracy for individual stars in such a program. Finally it is vital for this sort of observations that the 18 cm band is free of interference.

The phase lags calculated for the OH/IR stars from the Dwingeloo sample show that a new careful analysis was justified. Though we confirm their overall results, we think our estimates of phase lags and errors are more reliable than those published by Herman and Habing (1985b).

Further assumptions are required to calculate distances with this geometrical method. The first assumption of spherical symmetry seems to be satisfied within reasonable accuracy. But we also have to argue that our measurements of physical and angular size originate at the same distance from the star. This is not the same as spherical symmetry in a maser and this last assumptions is not easily checked.

With these restrictions in mind, we recalculate the distances of the stars in the Dwingeloo sample. We present an estimate of the error in the distance for the individual objects that reflects the observational errors.

In our new analysis the problems with the luminosities of these stars are no longer evident, but the luminosities are still very high compared with other samples of OH/IR stars. Several selection effects can account for this, but a possible bias cannot be ruled out.

Acknowledgements. We like to thank Harm Habing for continuous advice, a large number of students who carried out the observations with the DRT, Jaap Herman for very high quality data and Maarten Roos for help with the reduction.

The DRT is operated by NFRA, the Netherlands Foundation for Research in Astronomy. The NFRA receives its funds from NWO, the Netherlands Organisation for Scientific Research, H.J.v.L. acknowledges partial travel support from NATO grant No. 870547.

Appendix A: (co)variances of interchannel lag estimates

Consider one pair of channels, i and j, satisfying the assumptions of Sect. 2.4.2. We apply a sinc function interpolation to Eq. (12) and get

$$f_i(t)=s(t)+p_i(t),$$
$$f_j(t)=s(t-\tau_{ij})+p_j(t). \tag{A1}$$

$p_i(t)$ and $p_j(t)$ are uncorrelated white noise processes (bandwidth $1/2\Delta$, variances σ_i^2 and σ_j^2) and τ_{ij} is the interchannel lag. For convenience, we assume $\tau_{ij}=0$, without loss of generality. The estimate of τ_{ij} is obtained by shifting $f_i(t)$ relative to $f_j(t)$ and by determining the residue $R_{ij}(\tau)$:

$$R_{ij}(\tau)=\frac{1}{T}\int_0^T (f_i(t-\tau)-f_j(t))^2\,\mathrm{d}t, \tag{A2}$$

where $T=N\Delta$ is the time span of the observations. The i.c. lag estimate is the value of τ where $R_{ij}(\tau)$ is minimum, i.e.

$$\hat{\tau}_{ij}=\frac{-\dot{R}_{ij}(0)}{\ddot{R}_{ij}(0)}=\frac{\int_0^T (p_i(t)-p_j(t))\dot{s}(t)\,\mathrm{d}t}{\int_0^T (\dot{s}(t))^2\,\mathrm{d}t}. \tag{A3}$$

The first expression is obtained from a parabolic approximation of $R_{ij}(\tau)$ and the second by substitution of Eq. (A1) and application of the small error assumption.

An expression similar to (A3) can be written down for a second pair of channels, k and l. The covariance of the two estimates is

$$E(\hat{\tau}_{ij}\hat{\tau}_{kl})=\frac{\int_0^T\int_0^T \dot{s}(t)\dot{s}(t')E((p_i(t)-p_j(t))(p_k(t')-p_l(t')))\,\mathrm{d}t\,\mathrm{d}t'}{(\int_0^T (\dot{s}(t))^2\,\mathrm{d}t)^2}. \tag{A4}$$

The expectation in Eq. (A4) consists of four terms of the type

$$\delta_{ik}E(p_i(t)p_i(t'))=\delta_{ik}\sigma_i^2\,\mathrm{sinc}\left(\frac{t-t'}{\Delta}\right), \tag{A5}$$

since $p_i(t)$ is bandlimited white noise. Evaluation of Eq. (A4) thus gives

$$E(\hat{\tau}_{ij}\hat{\tau}_{kl})=(\delta_{ik}-\delta_{il})\alpha_i+(\delta_{jl}-\delta_{jk})\alpha_j \tag{A6}$$

where

$$\alpha_i=\sigma_i^2\left(\frac{1}{\Delta}\int_0^T (\dot{s}(t))^2\,\mathrm{d}t\right)^{-1}, \tag{A7}$$

which is Eq. (14) of the main text. The variances of an estimate follow from Eq. (A6) by taking $k=i$ and $l=j$, which gives Eq. (13) of the main text.

Appendix B: derivation of explicit expressions for $\hat{\tau}_0$

The errors ε_{ri} in Eq. (17) have a $(I-1)\times(I-1)$ covariance matrix $\boldsymbol{Q}$, the elements of which are given by Eq. (15). Writing $\boldsymbol{Q}$ down we find that it is of a particular form:

$$\boldsymbol{Q}=\boldsymbol{A}+\alpha_r\boldsymbol{e}\boldsymbol{e}^{\mathrm{T}}, \tag{B1}$$

where $\boldsymbol{A}$ is a diagonal matrix with elements $\alpha_1,\ldots,\alpha_I$ and where $\boldsymbol{e}$ is a vector with unit elements, $\boldsymbol{e}^{\mathrm{T}}=(1,\ldots,1)$.

Expression (B1) is a special form of $(\boldsymbol{A}+\boldsymbol{B}\boldsymbol{C}\boldsymbol{B}^{\mathrm{T}})$, for which the following identity holds.

$$(\boldsymbol{A}+\boldsymbol{B}\boldsymbol{C}\boldsymbol{B}^{\mathrm{T}})^{-1}=\boldsymbol{A}^{-1}-\boldsymbol{A}^{-1}\boldsymbol{B}(\boldsymbol{C}^{-1}+\boldsymbol{B}^{\mathrm{T}}\boldsymbol{A}^{-1}\boldsymbol{B})^{-1}\boldsymbol{B}^{\mathrm{T}}\boldsymbol{A}^{-1}. \tag{B2}$$

Application to Eq. (B1) gives

$$\boldsymbol{Q}^{-1}=\boldsymbol{A}^{-1}+\frac{\alpha_r}{1+\alpha_r\boldsymbol{e}^{\mathrm{T}}\boldsymbol{A}^{-1}\boldsymbol{e}}\boldsymbol{A}^{-1}\boldsymbol{e}\boldsymbol{e}^{\mathrm{T}}\boldsymbol{A}^{-1}. \tag{B3}$$

This expression is easily worked out since $\boldsymbol{A}$ is diagonal. Substitution into Eqs. (10) and (11) and some straightforward algebra leads to the expressions (18), (19) and (20) of Sect. 2.5.

References

Alcock, C., Ross, R.: 1986, *Astrophys. J.* **305**, 837
Baud, B.: 1981, *Astrophys. J. (Letters)* **250**, L79

Baud, B., Habing, H.J., Matthews, H.E., Winnberg, A.: 1981, *Astron. Astrophys.* **95**, 156
Booth, R.S., Kus, A.J., Norris, R.P., Porter, N.D.: 1981, *Nature* **290**, 382
Carter, J.C.: 1986, *Haystack Observatory Internal Report on "GLONASS observations"*
Chapman, J.M.: 1988, *Monthly Notices Roy. Astron. Soc.* **230**, 415
Chapman, J.M., Cohen, R.J., Norris, R.P.: 1984, *Monthly Notices Roy. Astron. Soc.* **207**, 149
Chapman, J.M.: 1985, Thesis, Victoria University of Manchester
Cohen, R.J.: 1989, *Reports on Progress in Physics* (in press)
De Jong, T.: 1983, *Astrophys. J.* **274**, 252
Diamond, P.J., Martinson, A., Dennison, B., Booth, R.S., Winnberg, A.: 1988, in *Radio wave scattering in the interstellar medium*, eds. J.M. Cordes, B.J. Rickett, C.D. Backer, American Institute of Physics, New York, p. 195
Diamond, P.J., Norris, R.P., Rowland, P.R., Booth, R.S., Nyman, L-A.: 1985, *Monthly Notices Roy. Astron. Soc.* **212**, 1
Edelson, R.A., Krolik, J.H.: 1988, *Astrophys. J.* **333**, 646
Elitzur, M., Goldreich, P., Scoville, N.: 1976, *Astrophys. J.* **205**, 384
Engels, D., Kreysa, E., Schultz, G.V., Sherwood, W.A.: 1983, *Astron. Astrophys.* **124**, 123
Gaskell, C.M., Peterson, B.M.: 1987, *Astrophys. J. Suppl. Ser.* **65**, 1
Goldreich, P., Scoville, N.: 1976, *Astrophys. J.* **205**, 144
Habing, H.J.: 1988, *Astron. Astrophys.* **200**, 40
Harvey, P.M., Bechis, K.P., Wilson, W.J., Ball, J.A.: 1974, *Astrophys. J. Suppl. Ser.* **27**, 331
Herman, J.: 1983, Thesis, University of Leiden, Chap. II
Herman, J., Baud, B., Habing, H.J., Winnberg, A.: 1985, *Astron. Astrophys.* **143**, 122
Herman, J., Habing, H.J.: 1985a, *Physics Report* **124**, 255
Herman, J., Habing, H.J.: 1985b, *Astron. Astrophys. Suppl. Ser.* **59**, 523
Herman, J., Isaacman, R., Sargent, A., Habing, H.J., 1984, *Astron. Astrophys.* **139**, 171
Heske, A., Forveille, T., Omont, A., Van der Veen, W.E.C.J., Habing, H.J.: 1989, *Astron. Astrophys.* (submitted)
Jewell, P.R., Webber, J.C., Snyder, L.E.: 1980, *Astrophys. J. (Letters)* **242**, L29
Jones, T.J.: 1987, in *Late stages of stellar evolution*, eds. S. Kwok, S.R. Pottasch, Reidel, Dordrecht, p. 3
Kendall, M.G., Stuart, A.: 1973, *The Advanced Theory of Statistics*, vol. 2, 3rd ed., Sect. 19.17, p. 91
Likkel, L.: 1989, *Astrophys. J.* **344**, 350
Netzer, N., Knapp, G.R.: 1987, *Astrophys. J.* **323**, 734
Olnon, F.M.: 1977, Thesis, University of Leiden
Paczinsky, B.: 1971, *Astron. Astrophys.* **21**, 417
Reid, M.J., Muhleman, D.O., Moran, J.M., Johnston, K.J., Schwartz, P.R.: 1977, *Astrophys. J.* **214**, 60
Röttgering, H.J.A.: 1989, *Astron. Astrophys.* **222**, 125
Schultz, G.V., Sherwood, W.A., Winnberg, A.: 1978, *Astron. Astrophys. (Letters)* **63**, L5
Steeman, F.W.M., Herman, J., Chapman, J.M., Cohen, R.J.: 1989 (in preparation)
Van der Veen, W.E.C.J., Habing, H.J.: 1988, *Astron. Astrophys.* **194**, 125
Van der Veen, W.E.C.J., Habing, H.J.: 1988, Thesis, Leiden, Chap. V
Van der Veen, W.E.C.J., Breukers, R.J.L.H.: 1989, *Astron. Astrophys.* **213**, 133